Mon. Not. R. Astron. Soc. **363,** 509–520 (2005) doi:10.1111/j.1365-2966.2005.09435.x

The gravitational and hydrodynamical interaction between the Large Magellanic Cloud and the Galaxy

C. Mastropietro,[1]★ B. Moore,[1] L. Mayer,[1] J. Wadsley[2] and J. Stadel[1]

[1]*Institute for Theoretical Physics, University of Zürich, CH-8057 Zürich, Switzerland*

[2]*Department of Physics and Astronomy, McMaster University, 1280 Main St. West, Hamilton, Ontario, L8S 4M1, Canada*

Accepted 2005 July 15. Received 2005 July 13; in original form 2004 December 22

ABSTRACT

We use high-resolution *N*-body/smoothed particle hydrodynamic simulations to study the hydrodynamical and gravitational interaction between the Large Magellanic Cloud (LMC) and the Milky Way Galaxy. We model the dark and hot extended halo components as well as the stellar/gaseous discs of the two galaxies. Both galaxies are embedded in extended cuspy ΛCDM dark matter haloes. We follow the previous 4 Gyr of the LMC's orbit such that it ends up with the correct location and orientation on the sky. Tidal forces elongate the LMC's disc, forcing a bar and creating a strong warp and diffuse stellar halo, although very few stars become unbound. The stellar halo may account for some of the microlensing events observed towards the LMC. Ram pressure from a low-density ionized halo is then sufficient to remove $1.4 \times 10^8\,M_\odot$ of gas from the LMC's disc, forming a great circle trailing stream around the Galaxy. The column density of stripped gas falls by two orders of magnitude 100 degrees from the LMC and the radial velocity along the trailing stream agrees well with the observations. The LMC does not induce any response in the Milky Way disc. On the contrary, the tides raised by the Milky Way determine the truncation of the satellite at about 11 kpc. After several gigayears of interaction, the gas disc of the LMC is smaller than the stellar disc due to ram pressure, and its size and morphology compare well with the observational data.

Key words: hydrodynamics – methods: *N*-body simulations – galaxies: interactions – Magellanic Clouds.

1 INTRODUCTION

The Milky Way–Magellanic Cloud system provides us with a close-up view of a complex ongoing galaxy interaction. Gravitational and hydrodynamical forces from the Galaxy are reshaping its largest satellites and creating the spectacular Magellanic Stream (MS). The MS is a trailing filament of neutral hydrogen that originates from the Magellanic Clouds and stretches for over ∼100 degrees in the Southern Sky and is the most prominent signature of an interaction between the Clouds and the Milky Way (MW). The combined interaction between these three galaxies must strongly influence the morphological evolution of the Clouds, as well as their internal kinematics and star formation history. A resonant interaction between the Galaxy and the Large Magellanic Cloud (LMC) could even be sufficient to excite the warp observed in the Galactic disc (Weinberg 1995, 1998).

Several models have been proposed in order to study the nature of this interaction and to isolate the main mechanism responsible for the formation of the MS. These models have become increasingly refined over the years. The first gravitational tidal models took into account just the binary interaction between the LMC and the MW (Lin & Lynden-Bell 1977; Murai & Fujimoto 1980), but later models included one or more close interactions between the Clouds themselves during the last orbit (Gardiner, Sawa & Fujimoto 1994; Lin, Jones & Klemola 1995; Gardiner & Noguchi 1996; Yoshizawa & Noguchi 2003; Connors et al. 2004; Bekki & Chiba 2005).

The strongest argument that has been used to argue for a tidal origin for the MS is provided by the discovery of neutral hydrogen in front of the LMC (Putman et al. 1998), although the amount of material in this feature is just a fraction of the mass of the MS (Putman et al. 2003a). However, there are some characteristics of the MS that tidal models cannot explain. In particular, they fail to reproduce the gradual decrease of the H I column density and the lack of a stellar tidal feature (Mathewson et al. 1979; Brueck & Hawkins 1983; Guhathakurta & Reitzel 1998). Stars are expected to be stripped by gravitational forces along with the gas, although Weinberg (2000) suggests that the stellar debris would have a different distribution respect to the gaseous MS and form a diffuse envelope around the LMC. Traces of the tidal interaction could be associated with the giant stars observed by Majewski et al. (1999) around the Magellanic Clouds.

★E-mail: chiara@physik.unizh.ch

A hydrodynamical interaction has also been invoked to explain the MS. Mathewson et al. (1987) proposed that gas is swept away from the intra-Cloud region and decelerated by random collisions with high-velocity clouds (HVC). This model requires unrealistic densities for the HVCs in the MW halo in order to justify the high number of encounters that should generate the MS and does not explain the column density gradient. Continuous stripping models (Meurer, Bicknell & Gingold 1985; Sofue 1994; Moore & Davis 1994) propose a scenario in which gas is stripped by ram-pressure forces from the outer regions of the Clouds through an interaction with a distribution of hot gas in the halo or an extended ionized disc. A satellite moving with a relative velocity v with respect to this external medium of density ρ experiences a pressure $P = \rho v^2$, which can be sufficient to remove part of the neutral gas from the disc. Together with the difficulties in creating a continuous leading arm – although the stripped material decelerated by ram-pressure forces could fall on smaller orbits and lead the Clouds (Sofue 1994; Moore & Davis 1994) – ram-pressure models are thought not to be able to reproduce the large amount of gas observed in the MS ($\sim 2 \times 10^8$ M$_\odot$ according to Putman et al. (2003a).

The presence of an extended hot halo surrounding the MW and in hydrostatic equilibrium within the dark matter potential is expected by current models of hierarchical structure formation (Maller & Bullock 2004). This gaseous halo, left over from the initial collapse, would be continuously fuelled by accretion of satellite galaxies over time. Recent observational results have confirmed the existence of a distribution of hot ($T \sim 10^6$ K) gas well beyond the Galactic disc, with a radius larger than 70 kpc in order to explain some ionization features discovered in the MS (Sembach et al. 2003; Putman et al. 2003b). Constraints from dynamical and thermal arguments fix the density of the gaseous halo in a range between 10^{-5} and 10^{-4} cm^{-3} at the LMC distance from the Galactic Centre. The Clouds are therefore subjected along their orbits to the ram pressure generated by a tenuous distribution of hot gas and the Magellanic system itself seems to be the result of a complex interaction that involves both hydrodynamical and tidal processes.

The aim of this work is to study for the first time the simultaneous effect of gravitational and hydrodynamical forces acting on the LMC as it moves within the Galactic halo, using fully self-consistent galaxy models. In particular, we are interested in the formation and evolution of the Magellanic Stream and in the dynamical changes in the internal structure of the LMC due to the interaction with the MW. We ignore the Small Magellanic Cloud (SMC) because of its small mass ($\sim$10 per cent of the LMC), neglecting the possibility of a close encounter between the two Clouds and the consequence of additional loss of mass. This approximation would lead to an underestimation of the amount of H I in the MS.

This paper is structured as follows. In Section 2 we present the main characteristics of the galaxy models that we use. The results of test wind tube simulations are discussed in Section 3. In Section 4 we analyse the results of the interacting runs regarding the MS and the LMC disc.

2 GALAXY MODELS

The initial conditions of the simulations are constructed using the technique described by Hernquist (1993). Both the Milky Way and the Large Magellanic Cloud are multicomponent systems with a stellar and gaseous disc embedded in a spherical dark matter halo. The density profile of the NFW (Navarro, Frenk & White 1997) halo is adiabatically contracted due to baryonic cooling (Springel & White 1999). Stars and cold ($T = 10^4$ K) gas in the disc follow the same exponential surface density profile of the form

$$\Sigma(R) = \frac{M_\mathrm{d}}{2\pi {R_\mathrm{d}}^2} \exp\left(-\frac{R}{R_\mathrm{d}}\right), \tag{1}$$

where M_d and R_d are the disc mass and radial scalelength (in cylindrical coordinates), respectively, while the thin vertical structure is characterized by the scaleheight $z_\mathrm{d} \sim \frac{1}{5} R_\mathrm{d}$:

$$\rho_\mathrm{d}(R, z) = \frac{\Sigma(R)}{2z_\mathrm{d}} \mathrm{sech}^2\left(\frac{z}{z_\mathrm{d}}\right). \tag{2}$$

The MW model comprises two further components: a stellar bulge and an extended hot gaseous halo. The bulge has a spherical Hernquist (Hernquist 1990) profile,

$$\rho_\mathrm{b}(r) = \frac{M_\mathrm{b}}{2\pi} \frac{r_\mathrm{b}}{r(r_\mathrm{b} + r)^3}, \tag{3}$$

where M_b is the bulge mass and r_b its scalelength.

Although the presence of an extended corona of hot gas seems to be the most likely explanation for the detection of O VI and O VII absorption lines associated with H I structures [Magellanic Stream, some high-velocity clouds, Outer Spiral Arm, Complex A, Complex C, according to Sembach et al. (2003)], its density structure is still uncertain, particularly at large distances from the Galactic Centre. These ionization features suggest a mean density of the gaseous halo (n_h) within 80 kpc of $\sim 10^{-4}$–10^{-5} cm^{-3} (Sembach 2003). Stanimirovic et al. (2002) provide similar values for the density at 45 kpc ($n_\mathrm{h} \lesssim 3 \times 10^{-4}$ cm^{-3}) in order to explain the confinement mechanism of the MS clouds through pressure support from the hot halo. Another constraint comes from the detection of Hα emission along the MS, which cannot be explained solely by photoionization from the Galactic disc (Putman et al. 2003b) and could be induced by the interaction with a relatively dense ($n_\mathrm{h} > 10^{-4}$ cm^{-3} at 50 kpc) gaseous environment (Weiner & Williams 1996). With a density higher than 10^{-4} cm^{-3}, Quilis & Moore (2001) are able to reproduce, using hydrodynamical simulations, the head–tail structure and the compression fronts associated with HVCs, in the case of either pure gas clouds or gas embedded within a dark matter halo. A significantly lower value for the upper limit of the halo density ($n_\mathrm{h} < 10^{-5}$ cm^{-3}) is found by Murali (2000) by requiring the survival of the cloud MS IV for 500 Myr against evaporation. However, we emphasize the fact that the evaporation time strongly depends on the temperature of the gaseous halo (Cowie & McKee 1977) and a choice of $T \sim 10^6$ K, three times lower than the value used by Murali, increases by almost a factor of 15 the lifetime of MS IV, making the survival of the cloud possible at a density of even 10^{-4} cm^{-3}. At larger distances from the Galactic Centre, constraints on the halo density are poor, although Blitz & Robishaw (2000) derive a value of 2.5×10^{-5} cm^{-3} at a distance of 200 kpc by applying ram-pressure stripping to dwarf spheroidal galaxies within the Galactic halo.

We model the hot halo with a spherical distribution of gas, which traces the dark matter profile within the virial radius and is in hydrostatic equilibrium inside the Galactic potential. Assuming an isotropic model, the halo temperature at a given radius r is determined by the cumulative mass distribution $M(r)$ of the dark, stellar and gaseous components of the MW beyond r and by the density profile $\rho_\mathrm{h}(r)$ of the hot gas:

$$T(r) = \frac{m_\mathrm{p}}{k_\mathrm{B}} \frac{1}{\rho_\mathrm{h}(r)} \int_r^\infty \rho_\mathrm{h}(r) \frac{GM(r)}{r^2}\, \mathrm{d}r, \tag{4}$$

where m_p is the proton mass, G and k_B are the gravitational and Boltzmann constants. The halo gas is completely ionized at a mean temperature of 10^6 K. We normalize the density profile using a hot

Table 1. Galaxy models. For each component, mass (in units of $10^{10}\,M_\odot$) and scale radius (kpc) are indicated. R_d and r_b are defined as in equations (1) and (3), while the scale radius of the NFW profile that characterizes both the DM and the hot halo is $r_s = r_{vir}/c$, where r_{vir} and c are the halo virial radius and concentration, respectively. The last three columns refer to high-resolution runs and report number of particles, particle mass (in units of $10^5\,M_\odot$) and softening length (kpc).

	Mass	Scale radius	N	m	ϵ
Milky Way Galaxy					
Bulge	0.73	0.70	10^4	7.3	0.1
Gaseous disc	0.46	3.53	10^5	0.46	0.1
Stellar disc	4.10	3.53	10^5	4.10	0.1
DM halo	104.0	18.2	10^6	10.4	0.5
Hot halo	1.0	18.2	5×10^5	0.20	0.5
Large Magellanic Cloud					
Gaseous disc	0.11	1.66	10^5	0.11	0.1
Stellar disc	0.11	1.66	5×10^4	0.22	0.1
DM halo	2.38	6.02	6×10^5	10.4	0.5

halo mass of $M_h = 10^{10}\,M_\odot$, which corresponds to a mean density of $2 \times 10^{-5}\,cm^{-3}$ within 150 kpc and 8.5×10^{-5} at 50 kpc. With the assumption that the gas traces the dark matter, we overestimate by a factor of 3 the ionized gas density near the disc; however, this is not important for the current study.

Our Milky Way model (Table 1) is similar to model A_1 of Klypin, Zhao & Somerville (2002) and was selected in order to match observational data at the present time. About 4 Gyr ago, when we start studying the evolution of the LMC, the dark and gaseous halo masses of the Galaxy may have been quite different. However, we expect that most of the dark halo mass was probably already in place at $z = 2$–3, since galaxy formation simulations suggest that large disc galaxies had the last major merger quite early in order for a large enough disc to form by $z = 0$. The evolution of the gaseous halo is poorly known, but work in progress suggests that its density could have been higher than the value adopted in this paper.

The masses and the scalelengths adopted for the LMC model (Table 1) reproduce quite well the peak of the rotation curves inferred by Kim et al. (1998) and van der Marel et al. (2002). As we will see in Section 4, the interaction with the MW does not affect significantly the stellar and dark matter mass in the inner 8–9 kpc of the LMC (which is the interval covered by H I and carbon star data) and consequently the global rotation curve within this radial range. In order to take into account the loss of cold gas from the disc of the satellite, we assumed an initial amount of gas in the disc that is ∼2–3 times larger than H I observed to be associated with the LMC (Kim et al. 1998; Putman et al. 2003a; Brüns et al. 2005).

Figs 1 and 2 show the rotation curves of the different components of the two galaxies. The concentration c and the spin parameter λ (Mo, Mao & White 1998) are indicated at the top left. The concentration is defined as $c = r_{vir}/r_s$, where r_{vir} and r_s are the virial and the scale radius of the NFW halo, whereas the spin parameter relates the angular momentum J and the total energy E of a halo with a virial mass M_{vir} through the relation

$$\lambda = J|E|^{1/2}G^{-1}M_{vir}^{-5/2}.$$

The disc of the satellite galaxy has, within the scale radius, a central mass surface density of $\sim 70\,M_\odot\,pc^{-2}$, which corresponds to a B-band surface brightness of ~ 23 mag arcsec^{-2}, if we adopt a mass-to-light ratio of 2.

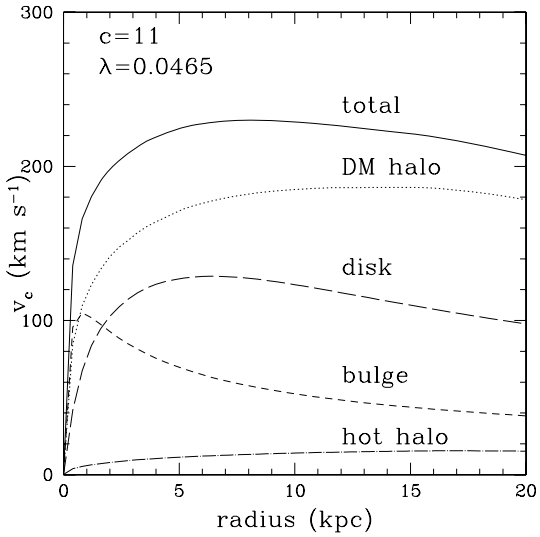

Figure 1. MW rotation curves. On the top left, spin and concentration parameter are indicated.

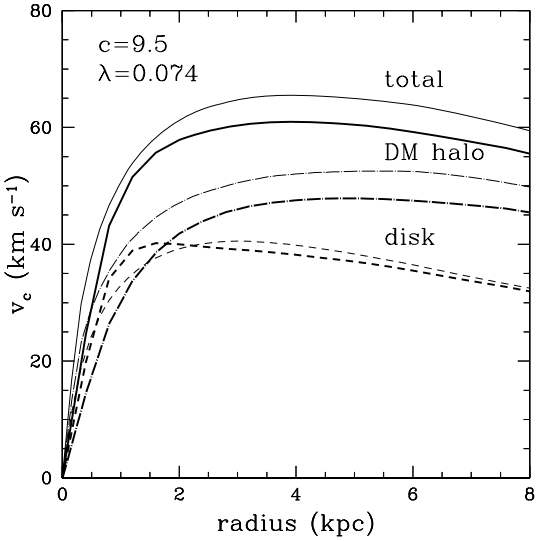

Figure 2. LMC rotation curves. Thin lines represent the rotation curves of the initial model, while thick lines refer to the satellite evolved for 4 Gyr in interaction with the MW. On the top left, spin and concentration parameter of the initial model are indicated.

The thickness of the discs is set such that Toomre's stability criterion (Toomre 1964) is satisfied, which requires, for a stellar disc,

$$Q_{star}(r) = \frac{\sigma_R k}{3.36 G \Sigma_s} > 1, \quad (5)$$

where σ_R is the radial velocity dispersion, k is the local epicyclic frequency and Σ_s is the stellar surface density. For a gaseous disc, equation (5) becomes

$$Q_{gas}(r) = \frac{v_s k}{\pi G \Sigma_g} > 1, \quad (6)$$

where v_s is the sound velocity and Σ_g is the surface density of the gas.

All the simulations we now discuss were carried out using GASOLINE, a parallel tree code with multistepping (Wadsley, Stadel & Quinn 2004). The high-resolution runs have 2.46×10^6 particles,

of which 3.5×10^5 are used for the discs and 5×10^5 for the hot halo of the MW (Table 1). The gravitational spline softening is set equal to 0.5 kpc for the dark and gaseous haloes, and to 0.1 kpc for stars and gas in the disc and bulge components. All the runs are adiabatic, except those treated in Section 4.2.1, which include radiative cooling.

3 TEST SIMULATIONS

The mass resolution of the simulations strongly influences the ram-pressure process. In particular, if the particles of the hot external medium are too massive, they do not flow smoothly on to the disc, but produce scattering and numerical holes, artificially increasing the stripping efficiency. In order to study these effects, we perform several test simulations in which we place the model LMC galaxy within a 'wind tunnel' and vary the mass of the hot halo particles for a fixed resolution of the LMC disc.

The first set (H1, H2 and H3) of runs simulates the passage of the satellite at the perigalacticon, which is the point along the orbit where ram pressure is most efficient due to the high values of $\rho_{\rm h}$ and v. The volume of the wind tunnel is an oblong of base equal to the diameter of the LMC and height $h = vt$, where v is the velocity of the satellite at the perigalacticon (250 km s^{-1}) and t is set at $\sim$2 Gyr (approximately the inferred orbital time for the LMC). We represent the hot gas as a flux of particles moving with a velocity v along the z-axis, parallel to the angular momentum of the disc. The hot particles have an initial random distribution, a temperature $T = 10^6$ K and a number density $n_{\rm h} = 8 \times 10^{-5}$ cm^{-3}. The box has periodic boundary conditions in order to restore the flow of hot gas that leaves the oblong. The disc particles have the same mass $m_{\rm disc}$ as in the high-resolution interacting runs (see Table 2), while the mass ratio with the particles in the oblong $m_{\rm h}/m_{\rm disc}$ is 1 : 10, 1 : 2 and 1 : 1. Gas is removed from the disc if the ram pressure produced by the hot halo of the MW is greater than the restoring force per unit area provided by the disc of the satellite. The condition for ram-pressure stripping is expressed by (Gunn & Gott 1972)

$$\rho_{\rm h} v^2 > 2\pi G \Sigma(R) \Sigma_{\rm g}(R), \qquad (7)$$

where v is the velocity of the galaxy with respect to the surrounding medium, $\rho_{\rm h}$ is the density of the hot halo of the MW and $\Sigma_{\rm g}\,(r)$ is the cold gas surface density at the radius R. Here Σ represents the gravitational surface mass density of the disc. The minimum radius given by equation (7) is the final stripping radius $R_{\rm str}$ beyond which the ISM can be removed from the galaxy. The halo component does not contribute to the restoring force initially, since in the case of a face-on impact any force associated to a spherical potential is perpendicular to the wind pressure. As the gas is stripped out from the disc in the z-direction, the disc gravity decreases while the projection of the radial halo gravity force in the z-direction rises (Schulz & Struck 2001). This effect is particularly important in the case of low ram-pressure regimes such as those in which we are interested. The condition for stripping expressed in equation (7) implicitly assumes instantaneous stripping from the disc and discrete ram-pressure stripping events such that the loss of mass approaches an asymptotic limit. If, instead, ram pressure is a continuous process with time-scales comparable with the orbital time of the satellite, the stripping radius calculated analytically underestimates the physical size of the gaseous disc. Such a continuous ram-pressure stripping occurs here not because of turbulent or viscous stripping but because the gas at the edge of the disc heats up responding to the compression exerted by the outer medium and can therefore become unbound by increasing its energy despite the ram-pressure wind being constant. Time-scales of both Kelvin–Helmholtz instabilities and artificial viscous forces are close to 10 Gyr because of, respectively, stabilization due to the cuspy halo potential of the LMC and the high mass resolution employed, and are therefore negligible over the time-scales explored here.

Equation (7) expresses the condition for stripping in the midplane of the disc, where the restoring force from the disc is maximum. In order to provide a numerical definition for the stripping radius, we can assume that particles that lie in the midplane of the disc are those included in a thin (with a thickness $\sim$2 softening lengths) layer parallel to the disc plane. We estimate $R_{\rm str}$ as the radius that contains 99 per cent of the LMC gas particles in the midplane of the disc. Thus we excluded a small fraction of particles located at large radial distance from the centre of the galaxy due to heating by the external hot medium. The mass of gas that remains in the disc can be computed by summing the disc particles inside a cylinder of radius $R_{\rm str}$ and thickness 1 kpc. The mass of gas bound to the satellite at a time t is instead not directly related to $R_{\rm str}$, but is determined by the potential of the dark halo. We calculate it balancing kinetic, thermal and potential energy in concentric spherical shells centred on the LMC, defining the gas tidal radius $r_{\rm g}$ as the radius of the most distant bound shell.

The mass of cold gas stripped from the LMC's disc $M_{\rm str}$ decreases as we decrease the mass of the halo particles: in run H1, $M_{\rm str}$ is $\sim$1.6 times larger than in H3 (Table 2). Mass resolution also determines the shape of the front edge and influences the morphology of the

Table 2. LMC wind tunnel simulations. For each run, the density $\rho_{\rm h}$ of the hot medium and the velocity v of the satellite are indicated. The resolution of each model is expressed in terms of the mass ratio $m_{\rm h}/m_{\rm disc}$ between halo and disc particles. N is the number of hot particles, while the last four columns give the ram-pressure stripping radius $R_{\rm str}$ and the mass stripped from the disc $M_{\rm str}$, the gas tidal radius $r_{\rm g}$ and the mass of gas unbound to the galaxy $M_{\rm unb}$. In the case of edge-on galaxies, the stripping radius $R_{\rm str}$ is the average value between the two sides of the disc. All the values are calculated at $t = 2$ Gyr.

Run	Model	$\rho_{\rm g}$ (10^{-5} cm^{-3})	v (km s^{-1})	$m_{\rm h}/m_{\rm disc}$	N (10^6)	$R_{\rm str}$ (kpc)	$M_{\rm str}$ (10^8 M$_\odot$)	$r_{\rm g}$ (kpc)	$M_{\rm unb}$ (10^8 M$_\odot$)
H1	face-on	8	250	10	0.37	4.0	4.11	6.7	2.84
H2	face-on	8	250	2	1.86	5.3	2.76	7.5	1.32
H3	face-on	8	250	1	3.2	5.5	2.52	7.8	1.0
L1	face-on	3.5	175	2	0.54	6.6	2.09	8.3	0.58
L2	face-on	3.5	175	1	1.07	6.8	2.02	8.5	0.44
L3	face-on	3.5	175	0.5	2.14	6.9	1.99	8.6	0.42
E1	edge-on	8	250	2	1.86	5.5	2.74	7.7	1.32
E2	edge-on	3.5	175	2	1.07	6.2	2.32	8.1	0.79

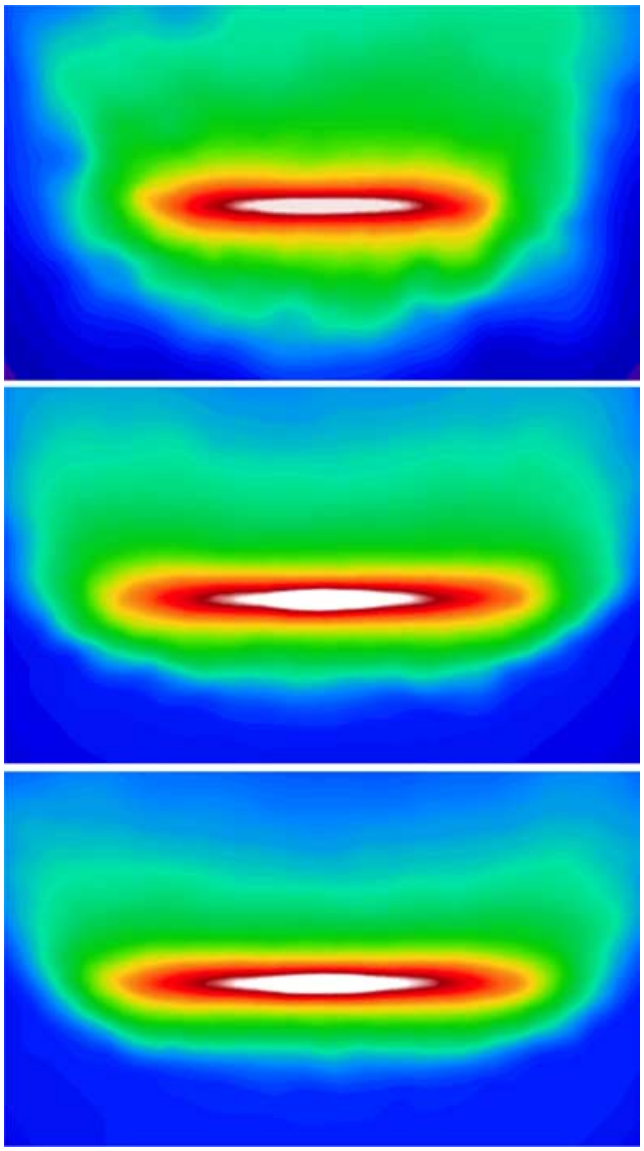

Figure 3. From top to bottom: column density distribution for the LMC test models H1, H2 and H3. The scale is logarithmic, with blue corresponding to the density of the hot halo gas. The effects of resolution are clearly apparent in the upper panel.

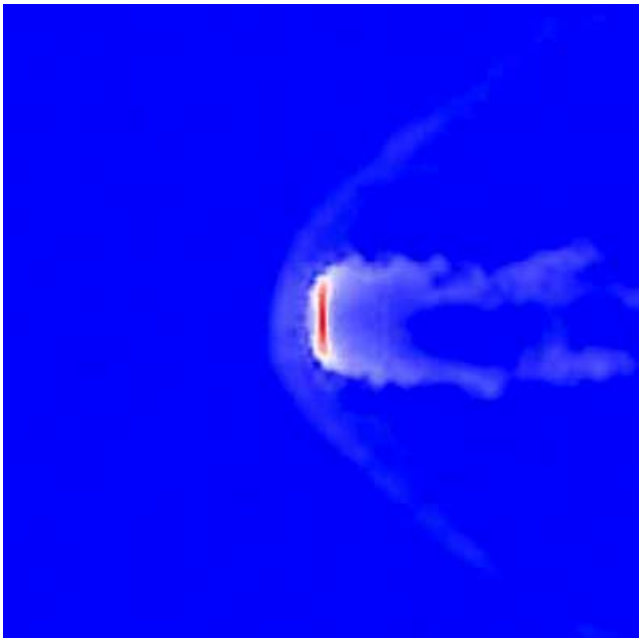

Figure 4. H3 run: density distribution of gas in a thin slice perpendicular to the LMC disc. The satellite is moving face-on towards the left, while a shock front forms in the external medium in front of the disc.

gaseous disc. Fig. 3 shows the gas density in the disc after 2 Gyr for the H1, H2 and H3 runs. Numerical effects in the low-resolution run are quite evident: the massive hot particles produce particle–particle interactions with gas in the galaxy, creating holes and discontinuities along the front edge of the disc. The spiral pattern is partially destroyed and the disc loses its symmetry. Scattering reduces the stripping radius by a factor of 1.4 and produces a sharp truncation, while the effect of pure ram pressure is much more gradual, since halo particles stream around the disc. Finally, the removed gas forms an asymmetric and turbulent tail. The high-resolution run H3 appears very symmetric, with a flat and uniform edge and a regular stream, which flows around the disc and creates a low-density region behind (Fig. 4). As previously noticed by several authors (Quilis, Moore & Bower 2000; Quilis & Moore 2001; Schulz & Struck 2001), a bow shock forms in front of the disc, increasing the local intracluster medium (ICM) temperature from 10^6 to 2.5×10^6 K. The intermediate run H2 is similar to H1, although the gas tail is more pronounced and the amount of stripped gas is less than 10 per cent larger. The resolution (mass ratio of 1 : 2) of the H2 run is to be a good compromise between the necessity of solving the gas dynamics and the number of particles to use in a full production simulation.

The runs L1, L2 and L3 have a gas density ($\rho_h = 3.5 \times 10^{-5}$ cm^{-3}) and satellite velocity (175 km s^{-1}) similar to our final LMC's orbit with apocentric distance ∼50 kpc and apo/perigalacticon ratio ∼ 2.5 : 1 (see Section 4.1). Reducing the ram pressure by a factor of 3 decreases the stripped mass by ∼20 per cent, while the amount of unbound gas is almost 60 per cent smaller. This indicates that a lower ram pressure is still efficient in stripping gas from the disc, but part of the removed material is now bound to the satellite by the dark halo gravity. The simulations were computed using three different resolutions, with m_h/h_{disc} equal to 2, 1 and 0.5. The stripped mass converges for $m_h/m_{disc} < 1$.

The dependence of ram pressure on the satellite orientation is not a simple function of the angle between the disc plane and the orbital velocity (Vollmer et al. 2001) and can depend on the ram pressure and the structure of the satellite (Abadi, Moore & Bower 1999; Quilis et al. 2000; Schulz & Struck 2001; Marcolini et al. 2003). In the simulations E1 and E2 the galaxy is moving edge-on through the hot gas. Comparing the amount of stripped mass of E1 and E2 with the results of the corresponding face-on runs H2 and L1, it is clear that the stripping is not very sensitive to disc orientation. This is consistent with the conclusions of Marcolini et al. (2003), who observe that ram-pressure stripping sensitively depends on the inclination angle of the disc only in regimes of strong winds. In the case of relatively large dwarfs (the LMC total mass lies between their models MD and LG) subject to weak ram-pressure forces, as in the MW halo case, the central region of the disc is essentially unaffected for any inclination of the galaxy and the outer parts are similarly stripped in face-on and edge-on runs. These results imply that the amount of gas in the MS will only slightly depend on the

initial inclination of the LMC disc and on the precession eventually induced by tidal forces from the MW.

4 INTERACTING RUNS

4.1 Orbital parameters

The morphology of the MS indicates that the orbit of the LMC is nearly polar and anticlockwise, as seen from the Sun, while kinematical data (van der Marel et al. 2002) imply that the present position at ∼50 kpc from the Galactic Centre is close to the perigalacticon. Since the mass ratio between the MW and its satellite is about 50 : 1, we expect that the effects of dynamical friction are not negligible on time-scales comparable with the orbital period. On the other hand, at each pericentric passage the LMC loses mass from tidal stripping, increasing its decay time: dynamical friction becomes less effective as the satellite approaches the Galaxy (Colpi, Mayer & Governato 1999).

Dynamical friction implies that we cannot precisely make a backwards integration of the LMC's orbit; therefore, we make several low-resolution test simulations (3×10^5 particles) in order to find the correct starting point for the LMC 4 Gyr in the past such that it ends up with the present distance, velocity and orientation on the sky. We find orbital parameters close to the ones obtained by Gardiner et al. (1994) and Gardiner & Noguchi (1996). In particular the orbital plane is perpendicular to the Galactic disc, the present eccentricity [defined as $(r_{\rm apo} - r_{\rm per})/(r_{\rm apo} + r_{\rm per})$, with $r_{\rm apo}$ and $r_{\rm per}$ the apogalacticon and perigalacticon distances] and the orbital period are, respectively, 0.44 and ∼2 Gyr. The orbital separation between the MW and the LMC is plotted in Fig. 5 for the past 4 Gyr and for 4 Gyr into the future. The satellite is currently at 50 kpc from the Galactic Centre and is moving away from the perigalacticon (at 45 kpc) with a modulus of the velocity of 250 km s^{-1}. Its local standard of rest (LSR) velocity $v_{\rm LSR}$, i.e. the radial velocity seen from the Sun, is 270 km s^{-1}, while the present position in Galactic coordinates is $(b, l) = (-30^\circ, 277^\circ)$. All these values are quite close to those provided by observations. In particular, the observed $v_{\rm LSR}$ is 274 km s^{-1} according to Luks & Rohlfs (1992) and Hardy, Suntzeff & Azzopardi (1989), while $(b, l) = (-32.89^\circ, 280.46^\circ)$ from Tully (1988). Fig. 5 evidences that the LMC orbit is slowly sinking, with each apogalactic distance ∼20 per cent smaller than the previous one. We will show in the next subsection that the change in the orbital parameters due to dynamical friction strongly affects the tidal forces and rate of ram-pressure stripping.

In choosing the initial inclination and position of the line of nodes, we make the approximation that they do not change during the interaction. In particular, we adopt the values from van der Marel et al. (2002): respectively $i = 34.7^\circ$ and $\Theta = 129.9^\circ$. This choice could partially influence the final stellar structure of the disc, but not the ram-pressure stripping process, as seen in the previous section.

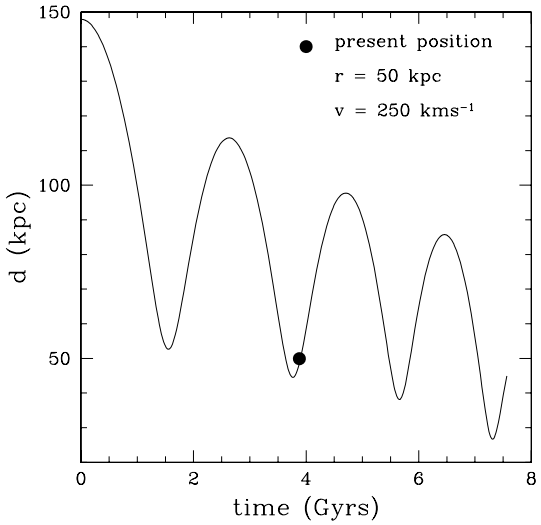

Figure 5. Orbital separation for the MW–LMC system.

4.2 The Magellanic Stream

The close interaction with the MW strongly perturbs the entire structure of the satellite. In particular, during the 4 Gyr preceding the present epoch, the LMC loses ∼80 per cent of its dark halo, and is currently tidally truncated at a radius of 11 kpc, consistent with the values provided by analytic calculations (Weinberg 2000; van der Marel et al. 2002) and with observations of the outer regions of the disc (Irwin 1991; van der Marel 2001). The contribution of the dark matter halo to the final rotation curve within 8 kpc from the centre decreases by ∼ 5 km s^{-1} and the disc component predominates in the inner region (Fig. 2).

While all the stars within the tidal radius are likely to be gravitationally bound, this is not true for gas. In fact, part of the gas that lies within the tidal radius can have enough thermal energy to escape from the potential well of the galaxy. Fig. 6 illustrates the evolution of the baryonic mass as a function of time. The dotted and solid curves refer to the stellar and gaseous components, respectively, while the dashed curve represents the gas within the tidal radius that is actually bound to the LMC.

After two perigalactic passages the satellite loses roughly ∼12 per cent of its gas and ∼4 per cent of stars. A pure tidal stripping model would remove similar amounts of both stars and gas unless the initial gas disc was significantly more extended. The larger amount of stripped gas is due primarily to ram-pressure stripping: the rate at which gas is lost increases as the LMC approaches perigalacticon (the solid vertical lines in the plot), corresponding to higher densities

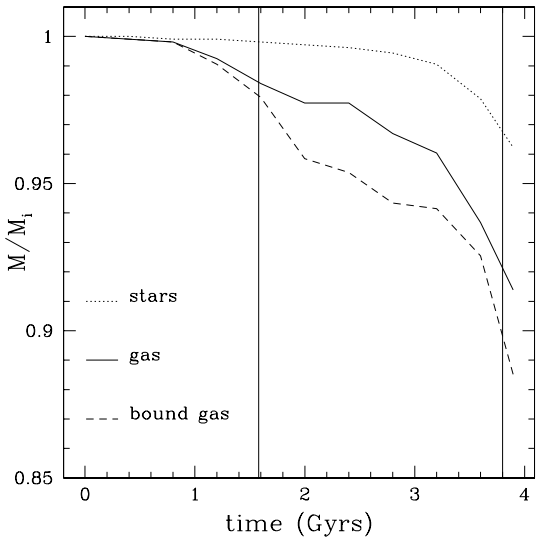

Figure 6. Fraction of stars and gas bound to the satellite during the last 4 Gyr. Both the gas within the tidal radius and the bound gas are plotted. $M_{\rm i}$ is the initial mass of each disc component. The vertical solid lines indicate the perigalactica.

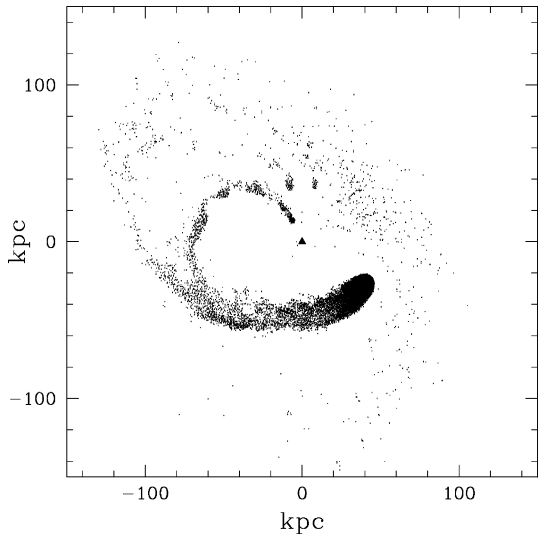

Figure 7. Final distribution of gas from the LMC disc in a plane perpendicular to the Galactic plane.

of the diffuse halo gas and to higher velocities of the satellite along the orbit.

Stars are stripped from the LMC only during the last perigalacticon, since the previous perigalactic passage is too far from the MW to produce significant tidal shocks and to perturb the stellar structure of the satellite. The present stellar distribution (see bottom part of Fig. 8) indicates that the disc is becoming elongated, forming a trailing and a small leading arm (with surface density $\sim 3 \times 10^{-3}\,\mathrm{M}_{\odot}\,\mathrm{pc}^{-2}$), but most of the stars stripped from the disc are still bound to the LMC and form a large spheroidal component.

Contrary to the stars, gas is stripped during the first passage at perigalacticon, forming a continuous stream that lies in a thin plane (width $\sim$25 kpc) perpendicular to the disc of the MW (Fig. 7) and between 50 and 75 kpc from the Galactic Centre. Fig. 8 (upper part) represents the distribution of stripped gas in an Aitoff projection. Our simulations predict that the MS forms a great polar circle, but most of the gas is lost recently and it is now at an angular distance between 10° and 120° from the LMC. The location of the MS in the Southern Galactic hemisphere is comparable with the values of b and l provided by observations. The material that lies in the Northern hemisphere was stripped from the satellite during the first orbit and is presently falling to the Galactic Centre. In particular the tail of this extended stream is intersecting the actual position of the satellite at $b \sim -30°$. It actually appears on the sky as a leading feature and could in principle reproduce observations of the leading arm of the Magellanic Stream. Its column density, however, is significantly lower than the observed one. The location of this gas is more clearly visible in Figs 9 and 10, which show a polar projection of the MS. Fig. 10 also indicates the hydrogen column density gradient along the MS, calculated assuming 72 per cent H I abundance. The gas in the 'leading region' presents a density peak between $b = -30°$ and $b = 30°$ and at $l \sim 285°$, but more material lies at larger longitudes and less negative latitudes, although the local density seems to be lower. Unfortunately, owing to the thermodynamical model adopted, the gas does not cool and condense in to individual clouds, but particles at the very end of the MS thermalize with the external hot medium, influencing both morphology and kinematics. Moreover, the resolution adopted in the simulation does not permit us to resolve this area with more than 10^3 gas particles.

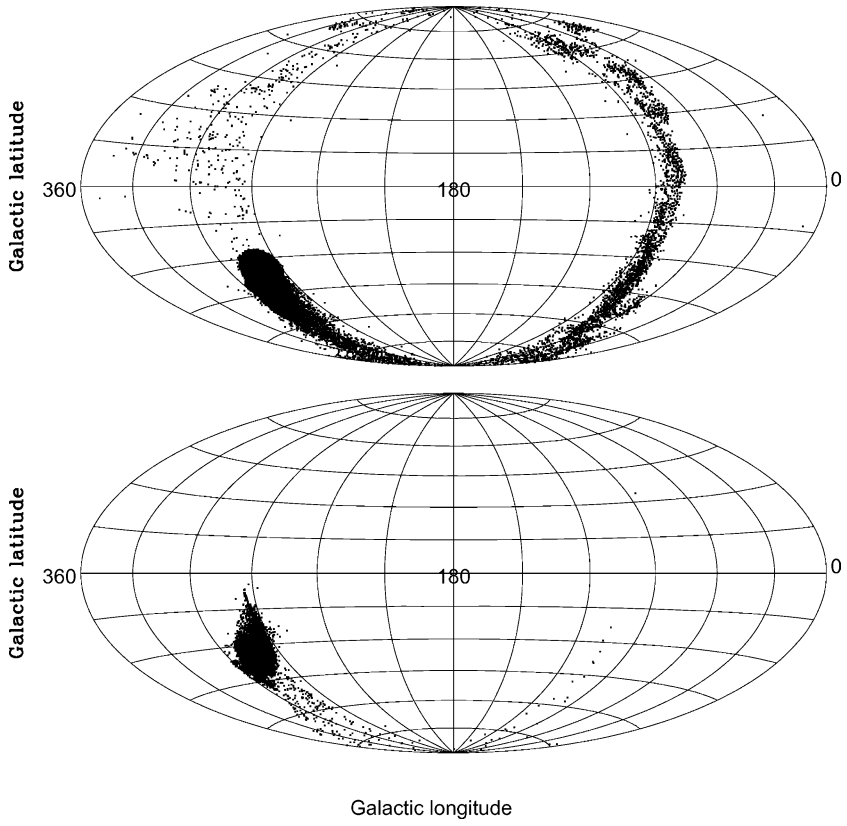

Figure 8. Present distribution of gas (top) and stars (bottom) from the LMC disc in Galactic coordinates.

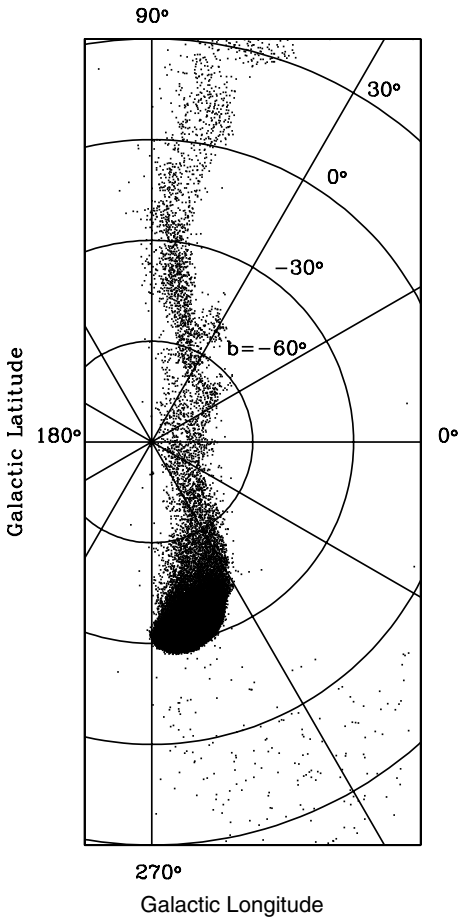

Figure 9. Polar projection of the simulated Magellanic Stream in Galactic coordinates.

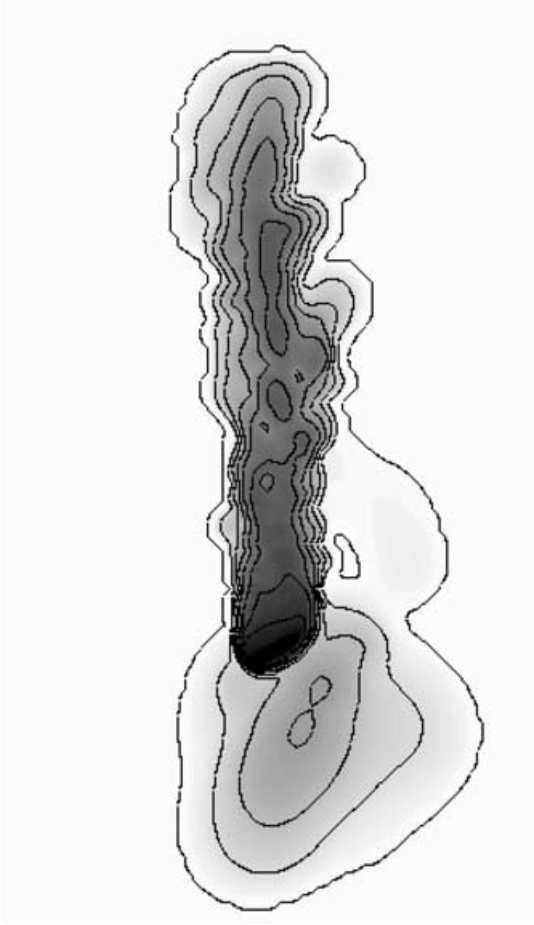

Figure 10. Hydrogen column density along the MS. Same projection and scale as in Fig. 9. The intensity values are on a logarithmic scale, with black corresponding to the highest dense regions within the LMC disc. The column density contours are 0.05, 0.15, 0.45, 1.35, 4.05, 12.15, 36.45 and 109.35 $\times$ 10^{19} cm^{-2}. The resolution limit in Putman et al. (2003a) is $\sim$2 $\times$ 10^{18} cm^{-2}, close to our second outermost level.

The column density of the gas located where we expect to find the trailing arm gradually decreases along the length of the MS moving from the LMC to (b, l) $\sim$ (20°, 80°). At a fixed angular distance from the LMC the structure of the MS is not uniform but has some well-defined high-density regions. Within 120° from the satellite the decrease in density is by nearly two orders of magnitude along the MS (Fig. 11) and is comparable with the gradient in column density observed in the trailing arm moving from the head of the MS (3.3 $\times$ 10^{19} cm^{-2} at an angular distance of $\sim$10° from the LMC) to MS VI (3.6 $\times$ 10^{18} cm^{-2}). This decrease in density is due to the combination of two factors. The gas close to the head of the MS is pulled from the disc during the last perigalacticon, when the stripping rate is maximum, whereas the tip is $\sim$1 Gyr old and corresponds to an apogalactic passage. Moreover, the tail is formed by the first material stripped from the outer and low-density regions of the exponential disc. This decrease in column density is a remarkable success for the ram-pressure scenario since tidal models generically produce streams with surface densities that fall off much more slowly (Moore & Davis 1994; Gardiner & Noguchi 1996).

The mass of the stripped gas (1.4 $\times$ 10^8 M$_\odot$, almost 90 per cent of which is within the same angular distance from the LMC covered by observations) is similar to the amount of neutral hydrogen in the MS observed by Putman et al. (2003a) (2 $\times$ 10^8 M$_\odot$). The total amount of unbound gas after 4 Gyr is comparable with the gas stripped in one orbital time from an LMC model in a test tube simulation with densities and velocities characteristic of a perigalactic passage. This means that the tidal forces acting on the satellite

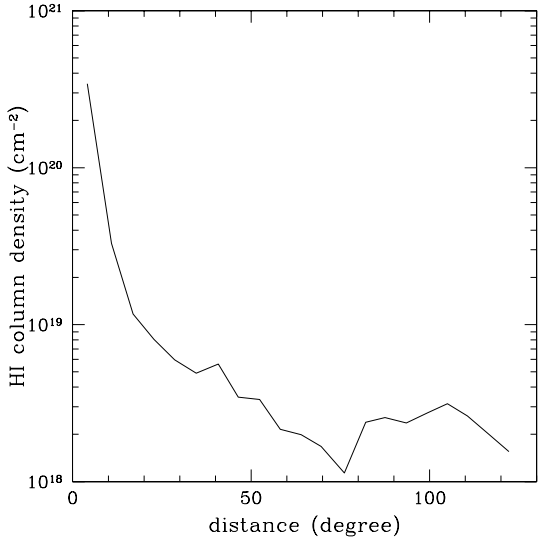

Figure 11. Hydrogen column density along the MS. The system of coordinates is chosen in order to have the LMC at 0 degrees.

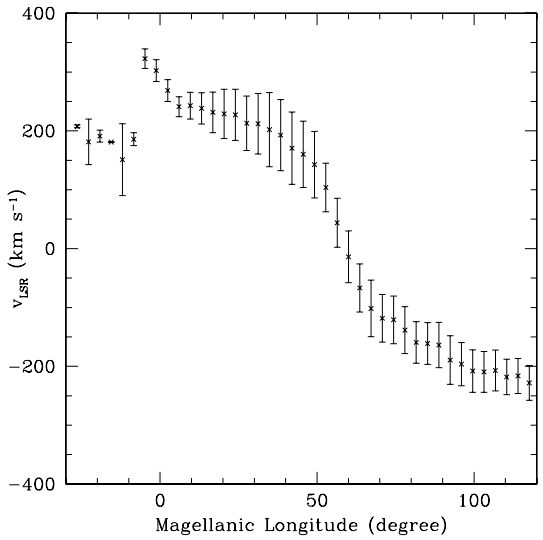

Figure 12. Radial velocity of the simulated MS in the local standard of rest as a function of the Magellanic longitude. Each point represents the mean velocity within an angular interval of 3.5° along the MS. The error bars show the standard deviation in each interval.

contribute to ram-pressure processes: as a consequence of the resulting asymmetrical potential and distorted stellar disc, it is easier to strip more gas from the LMC's disc since the gravitational restoring force is weaker. Thus even a low-density gaseous Galactic halo is able to remove a significant amount of gas from the LMC. The difference in the characteristic time-scales of hydrodynamical and gravitational forces explains why a gaseous leading arm does not form through tidal stripping: gas is removed quite early from the outer regions of the LMC disc, which during the second passage at the perigalacticon starts forming a leading arm feature.

Fig. 12 represents the LSR radial velocity of the MS versus the Magellanic longitude ($l_{\rm M}$) within an angular range similar to the one explored by observations (Putman et al. 2003a; Brüns et al. 2005). The Magellanic coordinate system adopted is the same as used by (Putman et al. 2003a) and previously described by Wakker (2001). The Magellanic longitude 0° corresponds to the centre of the LMC. The LSR velocity is calculated assuming a Solar circular rotation around the Milky Way of 220 km s^{-1}. The LMC is characterized by a mean radial velocity of 270 km s^{-1} (the steep increment of $v_{\rm LSR}$ around $l_{\rm M} = 0$ is due to the rotation of the LMC disc), while moving through larger Magellanic longitudes along the MS the velocity slows down to 0 km s^{-1} at ∼60° from the Cloud and to high negative values (∼ −250 km s^{-1}) at $l_{\rm M} \sim 120°$. The velocity gradient along the MS is almost 600 km s^{-1}, not far from the velocity range observed in HIPASS data [Fig. 12 could be compared with the analogous fig. 3 from Brüns et al. (2005)]. The points located at negative Magellanic longitudes represent the gas lying in the 'leading region'. The mean radial velocity of this area is ∼180 km s^{-1}, with a clear gap with respect to the velocity of the LMC, whereas the leading arm feature is observed at low relative velocities to the Cloud, with a mean $v_{\rm LSR}$ of 250 km s^{-1}. As we discussed previously, we do not expect to reproduce correctly the kinematics of this region since the gas is already thermalized with the hot surrounding medium.

4.2.1 Adiabatic versus cooling runs

We have presented results from simulations that do not include radiative cooling. As discussed in Section 3, in this case the gas in the disc of the LMC will increase its temperature as it is strongly compressed by the outer medium. In the adiabatic regime the gas can only lose energy by expansion, which requires a long time-scale, and can become easily unbound due to this input of thermal energy. We have run a simulation with radiative cooling adopting a standard cooling function for primordial gas (hydrogen and helium). The resolution is the same as in the high-resolution adiabatic interacting simulation. This run does not include star formation or supernovae feedback. The gas quickly heats up to ∼10^5 K due to shock heating, the peak of the cooling curve, then cools down on a time-scale much shorter than the dynamical time, shrinking in radius compared to its original location. After a few cycles of heating and cooling, the disc is significantly smaller and the gas sits deeper in the potential well and as a result no gas is stripped. However, what we are witnessing is probably the result of overcooling since we are neglecting the effect of star formation, namely heating from supernovae feedback and radiation from massive stellar associations. The LMC in particular shows widespread intense star formation across its disc and bar. In reality a multiphase interstellar medium (ISM) will result that will enable the gaseous disc to be in pressure equilibrium with the outer medium. Until we can effectively model this multiphase medium, we believe that the results of the adiabatic simulations are closer to reality.

4.3 The LMC disc

The Galactic disc remains unperturbed during the interaction, while the morphology of the satellite changes drastically. In particular, we will focus on the changes in the stellar and gaseous structure of the LMC.

Our initial model has a pure exponential stellar disc with a thin vertical structure and no bar component. After 4 Gyr from the beginning of the simulation, almost the entire stellar component is still bound to the satellite, but less than 90 per cent of the stars lie in the thin disc, which is surrounded by a stellar spheroid with a radius of ∼11 kpc (Fig. 13). The structure of this spheroidal component is quite complex, since a strong warp that wraps 180° around the LMC is superimposed on the underlying low-density stellar distribution. This final configuration is similar to the one obtained by Bekki & Chiba (2005). The warp forms after the first passage at the perigalacticon and involves a large fraction of the stellar particles. It extends ∼5 kpc out of the thin disc and is aligned with the major axis of the satellite. The existence of a warp is inferred by Kim et al. (1998) from the gas velocity field in the disc of the LMC, and by van der Marel & Cioni (2001) and Olsen & Salyk (2002) using the apparent magnitude of different classes of stars as a distance indicator. The diffuse spheroidal component has an average surface density of ∼5 × 10^{-2} $M_\odot$ pc^{-2}, which becomes one order of magnitude larger if we consider only the warp region. The warp deformation is partially directed along the line of sight and could have implications for the microlensing results, increasing the optical depth caused by self-lensing (Zaritsky & Lin 1997; Zhao & Evans 2000). The LMC's disc appears elongated, with a mean ellipticity $\epsilon = 0.38$ (where $\epsilon = 1 - q$ and q is the axial ratio), in a direction roughly aligned with the Galactic Centre and perpendicular to the MS. These values agree very well with the observations provided by van der Marel (2001). Within the inner 6–7 kpc of the model LMC a strong and asymmetric bar forms after the first perigalacticon.

The isodensity contours of the face-on disc were fitted with ellipses using the MIDAS task fit/ell3. The ellipse centres, ellipticity and major-axis position angle were considered as free parameters of the fitting procedure. The results of this projected analysis are

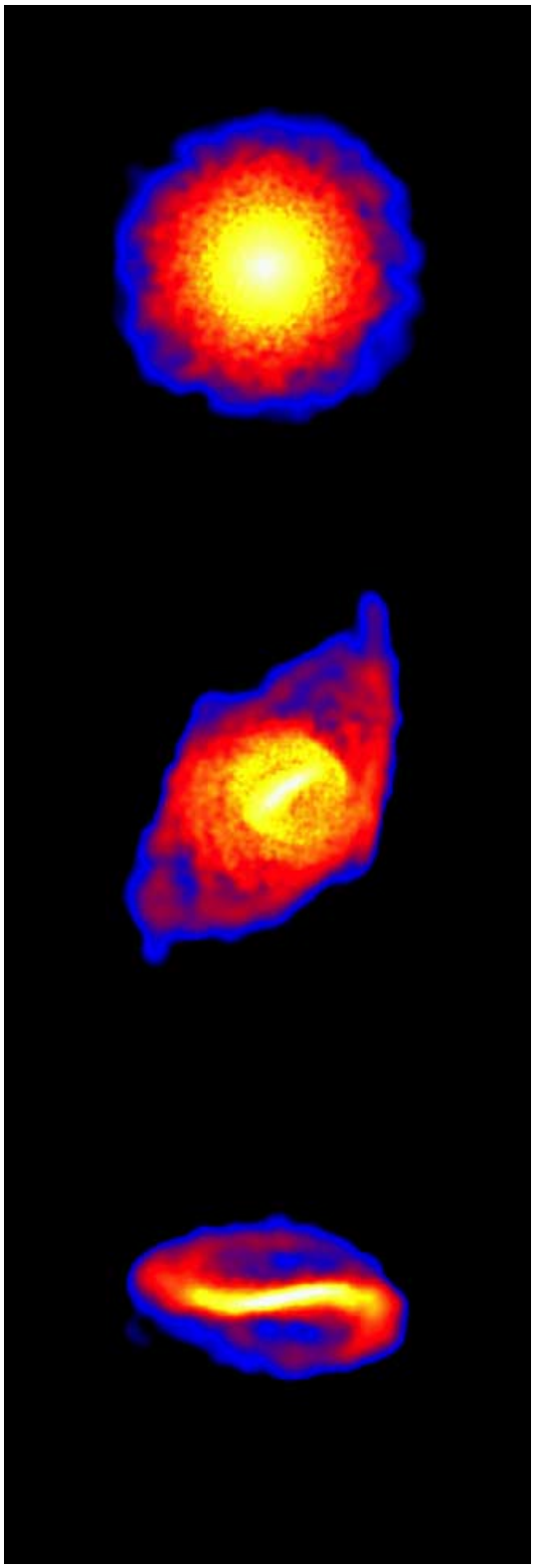

Figure 13. LMC stellar surface density. Colours represent a logarithmic scale, where white corresponds to a density of $10^2\,M_\odot\,pc^{-2}$ and blue to $10^{-2}\,M_\odot\,pc^{-2}$. From top to bottom: initial conditions, final face-on and edge-on projection. The bar and the strong warp are visible.

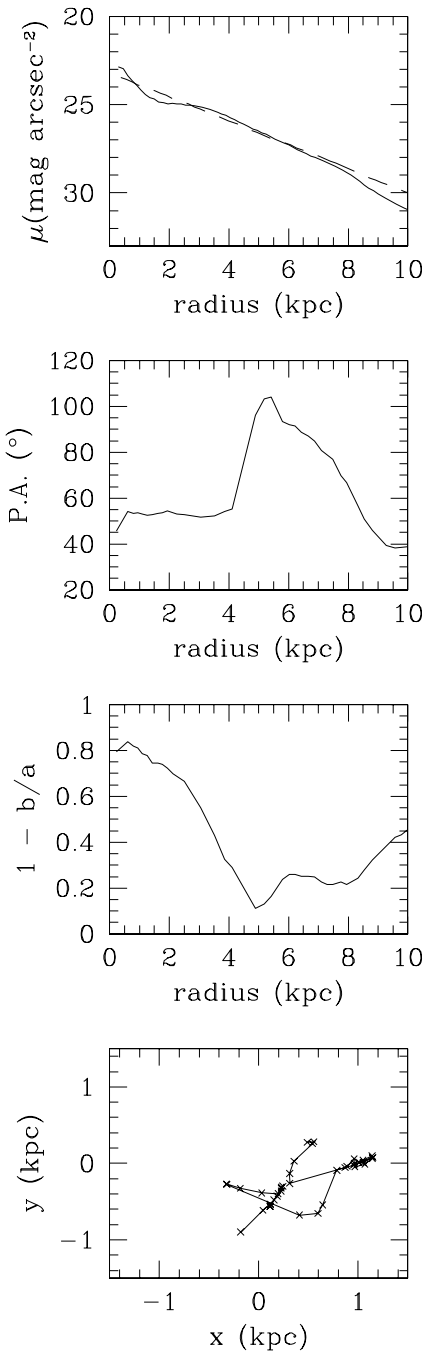

Figure 14. Photometric analysis of a face-on projection of the LMC disc. From top to bottom, the first three panels show *B*-band surface brightness, major-axis position angle and ellipticity profiles. The last plot represents the drift of the ellipse centre in the plane of the disc.

illustrated in Fig. 14. The top panel (solid line) shows the *B*-band surface brightness profile of the present face-on LMC, for which the best-fitting exponential curve has a scalelength of 1.5 kpc. The dashed line is the original exponential disc, with a scalelength of $\sim$ 1.7 kpc. The second and third panels illustrate the variation of the position angle and eccentricity as functions of radius. The position angle is almost constant in the central 4 kpc of the disc and presents a sharp twist beyond this radius, which corresponds to the transition between the bar region and the outer density contours characterized by ellipticities $\lesssim 0.2$. At radii $\gtrsim$8 kpc the disc appears more

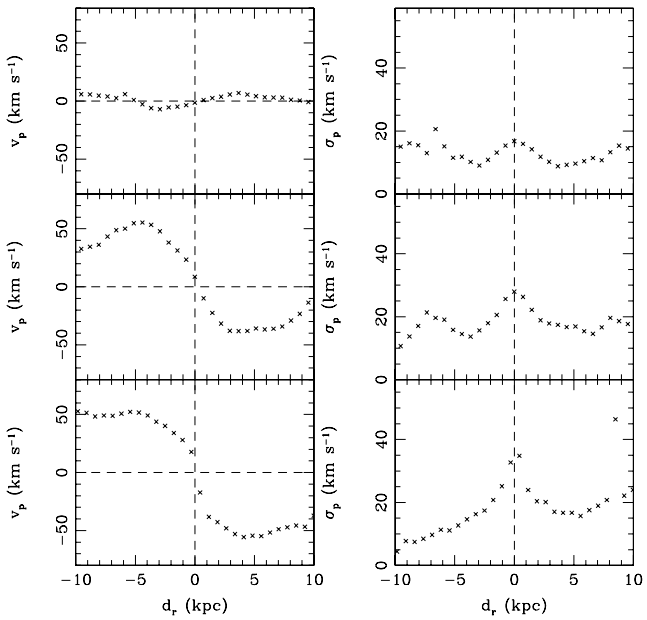

Figure 15. Projected velocity (left) and velocity dispersion (right) profiles for three different orientations of the LMC disc. From top to bottom: face-on, edge-on and end-on.

elongated, with a further increase in ellipticities and a twist of $\sim 50^{\circ}$ in the position angle. The bottom panel indicates the drift of the contour centres in the plane of the disc, which moves consistent with observations (van der Marel 2001) by almost 1 kpc.

Fig. 15 illustrates the kinematic profiles of three different orientations of the LMC disc observed today: from top to bottom, face-on, edge-on and end-on projections. The peak in the velocity dispersion in the central 6–8 kpc is mainly due to the bar formation, while the external regions appear to be dominated by a hot tidally perturbed component with $\sigma_{\rm p} \sim 20\,{\rm km\,s^{-1}}$.

The gaseous disc is completely dominated by stripping processes (Fig. 16). It retains a symmetric structure only within the central 12 kpc, in connection with the thin component of the stellar disc. Within this radius, we do not observe a significant displacement between the centre of the stellar distribution and the gaseous disc. The ram-pressure stripping radius after 4 Gyr is $\sim$6 kpc, a factor of 3 smaller than the initial disc radius and compatible with the results provided by HIPASS data (Putman, Gibson & Smith 1999).

5 CONCLUSIONS

We have carried out high-resolution gravitational/hydro-dynamical simulations of the interaction between the LMC and the Milky Way. As the LMC spirals inwards towards the Galaxy, it suffers ever-increasing gravitational tidal forces and hydrodynamical stripping. Our simulations cover the previous 4 Gyr of the orbit of the LMC such that at the final time it ends up at its correct location within the Galactic halo and with the observed inclination. We find that the combined effects of gravity and ram-pressure stripping can account for the majority of the LMC's kinematical and morphological features and the morphology of the Magellanic Stream.

Our model of the hot gaseous halo places a total of $10^{10}\,{\rm M}_{\odot}$ of ionized hydrogen within the dark matter halo of the Galaxy. The density at 50 kpc is $\approx 8 \times 10^{-5}\,{\rm atom\,cm^{-3}}$. This is sufficient to remove over $10^{8}\,{\rm M}_{\odot}$ of gas from the LMC, close to the observed mass of the MS, although the interaction between the LMC and the

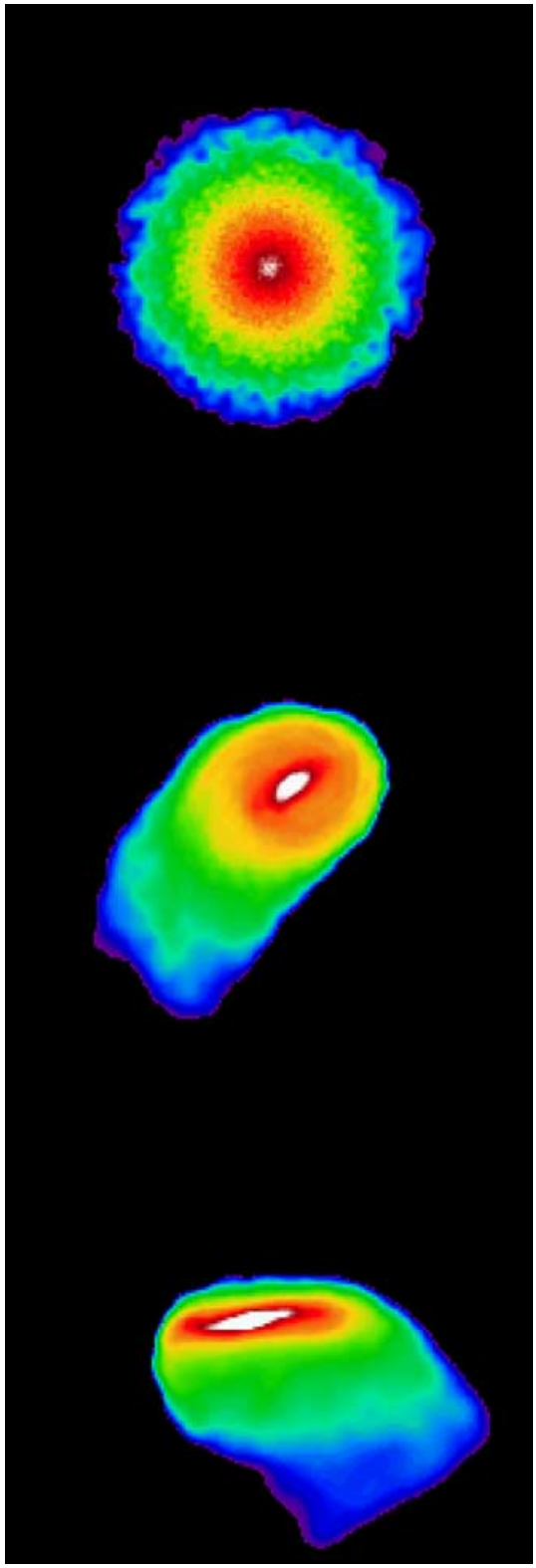

Figure 16. LMC gaseous column density. Colours represent a logarithmic scale, where white corresponds to a density of $10^{22}\,{\rm cm^{-2}}$ and violet to $10^{19}\,{\rm cm^{-2}}$. From top to bottom: initial conditions, final face-on and edge-on projection. The bar and the first part of the MS are visible.

Galaxy is probably not the only source of the MS gas. In fact, the complexity of the H I geometry in the region surrounding the Magellanic Clouds suggests that a close encounter between the Clouds and gas stripped from the SMC contributed not negligibly to the formation of the MS.

The gas stripped from the LMC disc forms a great circle, or a polar ring, around the Galaxy, consistent with the recently discovered extension of the MS into the Northern Hemisphere by Braun & Thilker (2004). Less material was stripped during the pericentric passage 4 Gyr ago since dynamical friction has moved the Clouds closer today. Thus we can reproduce the observed decrease in column density along the MS. Very few stars are tidally removed from the LMC, but its disc becomes severely warped due to the tidal interaction. This creates a diffuse halo of stars within the LMC that may have been observed as self-lensing events. The disc of stars is elongated by 2 : 1 oriented towards the Galactic Centre in agreement with the observations of van der Marel (2001).

Several improvements to our simulations could be made in order to study this fascinating interacting system in more detail: (i) more detailed modelling of star formation and the internal ISM of the LMC in order to study the role of gas stripping on star formation, and the role of star formation and the multiphase ISM on the stripping process; (ii) including the interaction with the SMC, which could supply a significant amount of gas to the MS and be responsible for the Magellanic bridge and the leading arm; and (iii) including a more realistic treatment of the gas physics in order to study the detailed structure of the stripped gas and its interaction with the halo gas as it infalls through the Galactic halo.

ACKNOWLEDGMENTS

We would like to thank Mary Putman, Tobias Kaufman, Andrea Macciò and Luigi Mancini for useful discussions. The numerical simulations were performed on the Zbox[1] supercomputer at the University of Zürich. CM is supported by the Swiss National Science Foundation.

REFERENCES

Abadi M. G., Moore B., Bower R. G., 1999, MNRAS, 308, 947
Bekki K., Chiba M., 2005, MNRAS, 356, 680
Blitz L., Robishaw T., 2000, ApJ, 541, 675
Braun R., Thilker D. A., 2004, A&A, 417, 421
Brueck M. T., Hawkins M. R. S., 1983, A&A, 124, 216
Brüns C. et al., 2005, A&A, 432, 45
Colpi M., Mayer L., Governato F., 1999, ApJ, 525, 720
Connors T. W., Kawata D., Maddison S. T., Gibson B. K., 2004, PASA, 21, 222
Cowie L. L., McKee C. F., 1977, ApJ, 211, 135
Gardiner L. T., Noguchi M., 1996, MNRAS, 278, 191
Gardiner L. T., Sawa T., Fujimoto M., 1994, MNRAS, 266, 567
Guhathakurta P., Reitzel D. B., 1998, in Zaritsky D., ed., ASP Conf. Ser. Vol. 136, Galactic Halos. Astron. Soc. Pac., San Francisco, p. 22
Gunn J. E., Gott J. R. I., 1972, ApJ, 176, 1
Hardy E., Suntzeff N. B., Azzopardi M., 1989, ApJ, 344, 210
Hernquist L., 1990, ApJ, 356, 359
Hernquist L., 1993, ApJS, 86, 389
Irwin M. J., 1991, in Haynes R., Milne D., eds., Proc. IAU Symp. 148, The Magellanic Clouds. Kluwer, Dordrecht, p. 453
Kim S., Staveley-Smith L., Dopita M. A., Freeman K. C., Sault R. J., Kesteven M. J., McConnell D., 1998, ApJ, 503, 674
Klypin A., Zhao H., Somerville R. S., 2002, ApJ, 573, 597
Lin D. N. C., Lynden-Bell D., 1977, MNRAS, 181, 59
Lin D. N. C., Jones B. F., Klemola A. R., 1995, ApJ, 439, 652
Luks T., Rohlfs K., 1992, A&A, 263, 41
Majewski S. R., Ostheimer J. C., Kunkel W. E., Johnston K. V., Patterson R. J., Palma C., 1999, in Chu Y.-H., Suntzeff N., Hesser J., Bohlender D., eds, Proc. IAU Symp. 190, New Views of the Magellanic Clouds. Astron. Soc. Pac., San Francisco, p. 508
Maller A. H., Bullock J. S., 2004, MNRAS, 355, 694
Marcolini A., Brighenti F., D'Ercole A., 2004, MNRAS, 352, 363
Mathewson D. S., Ford V. L., Schwarz M. P., Murray J. D., 1979, in Burton W.B., ed., Proc. IAU Symp. 84, The Large-Scale Characteristics of the Galaxy. Reidel, Dordrecht, p. 547
Mathewson D. S., Wayte S. R., Ford V. L., Ruan K., 1987, Proc. Astron. Soc. Aust., 7, 19
Meurer G. R., Bicknell G. V., Gingold R. A., 1985, Proc. Astron. Soc. Aust., 6, 195
Mo H. J., Mao S., White S. D. M., 1998, MNRAS, 295, 319
Moore B., Davis M., 1994, MNRAS, 270, 209
Mori M., Burkert A., 2000, ApJ, 538, 559
Murai T., Fujimoto M., 1980, PASJ, 32, 581
Murali C., 2000, ApJ, 529, L81
Navarro J. F., Frenk C. S., White S. D. M., 1997, ApJ, 490, 493
Nulsen P. E. J., 1982, MNRAS, 198, 1007
Olsen K. A. G., Salyk C., 2002, AJ, 124, 2045
Putman M. E. et al., 1998, Nat, 394, 752
Putman M. E., Gibson B. K., Staveley-Smith L., 1999, in Chu Y.-H., Suntzeff N.B., Jesser J.E., Bohlender D.A., eds, Proc. IAU Symp. 190, New Views of the Magellanic Clouds. Astron. Soc. Pac., San Francisco, p. 51
Putman M. E., Staveley-Smith L., Freeman K. C., Gibson B. K., Barnes D. G., 2003a, ApJ, 586, 170
Putman M. E., Bland-Hawthorn J., Veilleux S., Gibson B. K., Freeman K. C., Maloney P. R., 2003b, ApJ, 597, 948
Quilis V., Moore B., 2001, ApJ, 555, L95
Quilis V., Moore B., Bower R., 2000, Sci, 288, 1617
Schulz S., Struck C., 2001, MNRAS, 328, 185
Sembach K. R., 2003, in Colless M., Staveley-Smith L., Stathakis R., eds, IAU Symp. 216, Maps of the Cosmos. Kluwer, Dordrecht, p. 188
Sembach K. R. et al., 2003, ApJS, 146, 165
Sofue Y., 1994, PASJ, 46, 431
Springel V., White S. D. M., 1999, MNRAS, 307, 162
Stanimirovic S., Dickey J. M., Krčo M., Brooks A. M., 2002, ApJ, 576, 773
Taffoni G., Mayer L., Colpi M., Governato F., 2003, MNRAS, 341, 434
Toomre A., 1964, ApJ, 139, 1217
Toomre A., 1981, The Structure and Evolution of Normal Galaxies. Cambridge Univ. Press, Cambridge, p. 11
Tully R. B., 1988, Nearby Galaxies Catalog. Cambridge Univ. Press, Cambridge, p. 221
van der Marel R. P., 2001, AJ, 122, 1827
van der Marel R. P., Cioni M. L., 2001, AJ, 122, 1807
van der Marel R. P., Alves D. R., Hardy E., Suntzeff N. B., 2002, AJ, 124, 2639
Vollmer B., Cayatte V., Balkowski C., Duschl W. J., 2001, ApJ, 561, 708
Wadsley J. W., Stadel J., Quinn T., 2004, New Astron., 9, 137
Wakker B. P., 2001, ApJS, 136, 463
Weinberg M. D., 1995, ApJ, 455, L31
Weinberg M. D., 1998, MNRAS, 299, 499
Weinberg M. D., 2000, ApJ, 532, 922
Weiner B. J., Williams T. B., 1996, AJ, 111, 1156
Yoshizawa A. M., Noguchi M., 2003, MNRAS, 339, 1135
Zaritsky D., Lin D. N. C., 1997, AJ, 114, 2545
Zhao H., Evans, N. W., 2000, ApJ, 545, L35

[1] http:/www.theorie.physik.unizh.ch/stadel

This paper has been typeset from a TEX/LATEX file prepared by the author.